~~RAB35 SITS AT THE STEERING WHEEL OF CHEMOTACTICALLY MOVING CELLS~~

A RAB35-p85/PI3K AXIS CONTROLS OSCILLATORY APICAL PROTRUSIONS REQUIRED FOR EFFICIENT CHEMOTACTIC MIGRATION

Corallino Salvatore[1], Chiara Malinverno[1], Beate Neumann[2], Christian Tischer[2], Andrea Palamidessi[1], Emanuela Frittoli[1], Magdalini Panagiotakopoulou[5], Andrea Disanza[1], Gema Malet-Engra[1], Paulina Nastaly[1], Camilla Galli[1], Chiara Luise[4], Giovanni Bertalot[4], Salvatore Pece[4], Pier Paolo Di Fiore[1,3,4], Nils Gauthier[1], Aldo Ferrari[5], Paolo Maiuri[1], Giorgio Scita[1,3].

[1] IFOM, the FIRC Institute of Molecular Oncology, Via Adamello 16, 20139, Milan, Italy

[2] Advanced Light Microscopy Facility, European Molecular Biology Laboratory, Meyerhofstr. 1, 69117 Heidelberg, Germany

[3] DIPO, Department of Oncology and Hemato-Oncology, University of Milan, Via Festa del Perdono 7, 20122 Milan, Italy.

[4] Molecular Medicine Program, European Institute of Oncology, Via Ripamonti 435, 20141, Milan, Italy

[5] ETH Zurich, Laboratory of Thermodynamics in Emerging Technologies Sonneggstrasse 3,8092 Zurich, Switzerland

Correspondence to: Giorgio.scita@ifom.eu

ABSTRACT

How cells switch from a sessile to motile state and move chemotactically remains a major unmet challenge in cell biology. Emerging evidences indicate that for interpreting noisy, shallow gradients a system must behave as an excitable process. Through an RNAi-based, multi-step, high-content screening approach targeting mammalian RAB GTPases, we identified RAB35 as necessary for the formation of growth factors (GFs)-induced waves of Circular Dorsal Ruffles (CDRs), apically restricted actin-rich migratory protrusions. RAB35 is sufficient to induce recurrent and polarized CDRs that travel as oscillating and propagating waves, thus behaving as an excitable system that can be biased to control cell steering. Consistently, RAB35 is essential for promoting directed 1D and 2D chemotactic migration and 3D chemoinvasion of various cells in response to gradients of motogenic GFs. Molecularly, RAB35 does so ~~independently from its endocytic function, but~~ by directly regulating the activity of p85/PI3K~~/AKT~~ polarity axis. We propose that RAB35 is a novel molecular determinant for the control of an excitable, oscillatory system that acts as steering wheel for GF-mediated chemotaxis and chemoinvasion.

INTRODUCTION

Cells and particularly tumour cells use different motility modes to disseminate [1]. Each of these modes is driven and controlled by distinct molecular pathways, the nature of which remains largely unexplored. In one such strategy, referred to as "mesenchymal motility", single cells may detach from the tumour mass and advance as individual, invasive units [2]. One of the first steps of mesenchymal migration and invasion, particularly in response to growth factors stimulation, is the acquisition of a front-to-back polarity, which is driven by the extension of different kind of actin-based migratory protrusions, including canonical actin rich flat lamellipodia, small finger-like filopodia [3, 4], sausage-like lobopodia [5], blebs [6] and the poorly studied apically localized circular dorsal ruffles (CDRs) [7]. The latter structures are far less understood and their contribution and functional role in promoting cellular locomotion remains ill defined. This notwithstanding, CDRs have been proposed to be markers of cellular transition from amoeboid to mesenchymal migration [8]. In addition, these structures are sites of growth factor-induced macropinocytic internalization and have been shown to promote the endocytosis of various membrane bound molecules including EGF [9] and non-ligand engaged β3 integrin [10]. In the latter case, the internalization of the adhesion receptor is followed by its subsequent delivery to focal contacts and adhesions at the expanding leading edge, promoting directional motility [10]. Among the growth factors known to elicit robust and directional migration, HGF in epithelial cells [11] and PDGF [12, 13] in fibroblasts, have also been shown to be potent and specific inducer of CDRs [7]. This set of finding together with the observations that CDRs form rapidly, frequently in a recurrent wave-like pattern [14], suggests that these structures may operate as an oscillating device or steering wheel in driving chemotactic motility. It follows that factors controlling their formation might be critical chemotactic sensor or regulator and promoter of a directional, mesenchymal mode of motility by specifically controlling GF-mediated cell steering.

Methods

Details of the methods and statistics are described in supplementary information.

RESULTS and DISCUSSION

RAB35 is essential for CDRs formation.

We used CDRs as a read out for an RNAi-based phenotypic screening to identify new critical players promoting their formation and set out to test whether they are acting as oscillating waves steering cells during chemotaxis.

Given the involvement of CDRs in endocytic processes [10, 11, 15, 16], we specifically targeted each of the mammalian members of the RAB GTPase family, which includes more than 60 independent genes [17]. RAB GTPases, by controlling key steps of endocytosis and vesicular trafficking, are necessary for the execution of actin-based polarized functions that are in turn essential for cell migration and invasion [17, 18]. We devised a multistep screening strategy. For the primary screening, we used Mouse Embryonic Fibroblasts (MEFs) as model system because in response to PDGF stimulation the large majority of cells form easily detectable and prominent CDRs that appear in a highly synchronous, temporal fashion (with a peak after 10 min of stimulation). We employed a custom siRNA library, targeting all the members of the family (about 60 genes using 3 individual siRNAs for each gene, Table 1), arrayed onto 96-well imaging plates. We developed a fluorescence-based imaging pipeline to automatically monitor and quantitatively score the formation of CDR in PDGF-stimulated MEFs (for details see methods and Figure S1A-C). The accuracy of our pipeline was evaluated by manually/visually inspecting a sub-set of randomly chosen images in order to measure the ability to correctly recognize CDRs. The True Positive and False Positive rate of CDR recognition were 0.94 and 0.23, respectively. Raw data were quality controlled by removing images with a low number of nuclei (in all these cases the corresponding siRNA was considered as "inconclusive/cytotoxic") and by discarding out of focus images. In addition, we systematically evaluated plates based on the transfection efficiency of our cells (~ 80 %) that was measured by counting the percentage of polylobed nuclei upon *Incenp* down-regulation (Fig. S1C). Finally, the efficiency in forming CDRs was normalized in each experimental condition with respect to the negative control (siEGFP) of the screening (see methods) to obtain a CDR-score that was used to rank the various treatments (Fig. 1A). The top regulator of CDRs included, as expected, the β isoform of the PDGF Receptor, and few RAB GTPases, among which RAB35, the silencing of which resulted in one of the most robust inhibition of CDRs formation (Fig. 1A and Table 2). Next, we performed an independent secondary validation step by focusing on those genes for which at least 2 out of 3 siRNAs resulted in a CDR score < 0.4 (Table 2). Gene silencing in these cases was verified by quantitative-RT-PCR analysis (Fig. 1B). The silencing of RAB35, RAB8A and RAB8B resulted in a robust and reproducible decreased in CDR activity, thus

corroborating the validity of the primary screen and providing evidence that RAB35 is the main regulator of CDR formation among the mammalian RAB protein family (Fig. 1B).

To prove that the CDR-phenotype associated with RAB35 silencing is the result of specific targeting of the gene and rule out off-target effects, we performed a rescue experiment. To this end, we generated a population of MEF cells expressing the HA-tagged human form of RAB35, which is resistant to the murine oligo used to induce the silencing of the endogenous gene product, in a doxycycline-inducible fashion. Cells interfered for endogenous RAB35 displayed reduced CDR formation, which was fully rescued by the expression of the human protein (Fig. 2A). Of note, ectopically expressed RAB35 was diffuse on the cytoplasm and present on the plasma membrane, but re-localized to CDRs following stimulation with PDGF (Fig. S1D).

In addition to be migratory, CDRs are also sites of macropinocytic internalization [19]. Real-time phase contrast microscopy, consistently, revealed the formation of large fluid-filled, vesicle-like structures that invariably form following CDR closure (Movie 1). This was mirrored by PDGF-mediated increase in the internalization of large molecular weight, fluorescently-labeled Dextran, a "*bona fide*" macropinocytosis cargo. Importantly, MEFs stably down-regulated for RAB35 were severely impaired in the internalization of Dextran (Fig. 2B), reinforcing the notion that this GTPase is critical for CDRs formation and their endocytic functional activity.

We further validated our finding in a different cellular context. We used HeLa cells, which are of epithelial origin and form CDRs in response to HGF stimulation [20]. Silencing of RAB35 in these cells severely decreased CDRs formation as compared to scrambled-transfected cells (Fig. S1E), indicating that RAB35 is a critical regulator of CDR formation in response to different GF-dependent signaling pathways.

Finally, to establish whether RAB35 is also sufficient to induce these structures, we monitored by time-lapse phase contrast microscopy MEF cells expressing HA-RAB35 in a doxycycline-inducible fashion cultured in growing media without any addition of growth factors. Importantly, up-regulation of RAB35 was sufficient to promote the formation of multiple CDRs that display a persistent and rapid dynamics, as confirmed by the quantification of the number of events per cell monitored in one hour (Fig. 2C and Movie 2). This was mirrored by an increased rate of fluorescently-labeled Dextran internalization (Fig. 2D)

Collectively, these findings identify RAB35 as a non-previously characterized RAB GTPase essential for the formation of CDRs in response to stimulation with various growth factors.

RAB35-controlled CDRs act as cell steering, oscillating devices in response to directional cues.

CDRs play a key role in cytoskeleton remodeling associated with the transition from sessile to motile states [7]. In addition they frequently, if not invariably, form in close proximity to the cell leading edge [21], and are capable of initiating endo/exocytic cycles of plasma membranes and integrins that are subsequently delivered in a polarized fashion to the prospective lamellipodia [9, 10, 22, 23]. These properties suggest that CDRs may function as "*bona fide*" cellular steering compasses to initiate forward and directional chemotactic migration. Given the relationship between CDRs, cell locomotion and cell guidance, we further hypothesize that RAB35 by controlling their formation may also be essential for regulating directional, chemotactic motility.

To act as steering devices CDRs must form in a polarized fashion in response to local gradient of chemotactic growth factors, and their dynamics formation should be spatiotemporally correlated with the extension of lamellipodia protrusions. In addition, structural components and biochemical wiring involved in cell migration guidance are often behaving as excitable oscillatory systems, which may become spatiotemporally biased following chemoattractant exposure [24]. The propagation of actin waves at the ventral surface of neutrophil is a typical case in point [25-28]. We verified whether CDRs display all these features. Firstly, we monitored by time-lapse microscopy their formation and recorded the subsequent extension of lamellipodia in response to local delivery of PDGF. CDRs formed in polarized directions and their appearance/disappearance was followed by the subsequent extension of flat lamellipodia-like protrusions following the local delivery of PDGF (Fig. 3A and Movie 3). The temporal correlation between CDR and leading-edge protrusions was robust in RAB35-expressing cells. RAB35-expressing, but not control cells, form multiple CDRs in the absence of any added growth factor and these structures precede the extension of lamellipodia with a lag phase of about 105 sec (Fig. 3B and Movie 4). We further exploited the ability of RAB35 to induce a constitutive wave of recurrent multiple CDRs to characterize their overall dynamics in more details and relate it to the extension of membrane protrusions. We observed the following peculiar kinematic features: i) *travelling CDR waves*: in this case, CDR formed at the rear of an elongated, spatially restricted pseudopodia–like protrusion and move persistently along and in synchrony with the extended protrusion, with nearly identical speed (Fig. 3C and Movie 5); ii) *multiple CDRs expanding centrifugally:* a series of multiple and iterative CDR waves that form in diverse, but generally peripheral positions invariably expanding centrifugally toward the cell edge (see Movies 4); iii) *recurrent oscillating CDR waves*: recurrent CDRs that repeatedly form in the same location expanded and enclosed with a typical oscillatory frequency of about 20 min (Fig. 3D and Movie 6). Collectively, these features support the notion that CDRs behave as an excitable system of propagating waves, which can be biased by exogenously added PDGF to promote cell steering and chemotactic motility [24].

If CDRs are indeed *bona fide,* excitable, steering devices, their perturbation should impair directional motility, particularly toward growth factors known to induce robustly their formation right at the onset of chemotaxis. To this end, we first measured the ability of MEFs to migrate through a micro porous membrane towards a PDGF gradient in a Boyden chamber assay. Scrambled and RAB35-silenced cells (we used three independent siRNAs) were seeded into Transwell chambers. After 20 hours, cells on the top of the membrane were scraped away and the ones migrated at the bottom were stained with Crystal violet. An additional time point was taken 3 hours after cell plating to demonstrate that we seeded an equal number of cells, which display similar adhesion efficiency across all the different experimental conditions. The loss of RAB35 significantly and robustly reduced the number of cells crossing the porous filter by chemotaxis (Fig. 4A). To monitor MEF chemotaxis in real time and to explore the potential underlying cellular alterations, we employ a microfluidic commercial device that generate a stable linear gradient of PDGF. We used the ImageJ plugin "Chemotaxis tool" to extract migratory parameters, including forward migration index (chemotaxis) and mean velocity. Silencing of RAB35 significantly impaired chemotaxis and reduced mean cell velocity (Fig. 4B and Movie 7).

To understand whether the altered migratory capability observed upon RAB35 ablation is an intrinsic defect in the molecular machinery sustaining cell locomotion, we also monitored the migratory behavior of sparsely seeded Ctrl and short hairpin–silenced RAB35 cells in the absence of any external guiding factor in a random migration assay. Under these conditions, we found that RAB35 loss caused a significant but marginal decrease in cell velocity and had no effect on the formation of lamellipodia protrusions, suggesting that the machinery generating locomotory forces was not strictly dependent on RAB35 (Fig. 4C and Movie 8). On the contrary, the stable up-regulation of RAB35, which promoted that extension of multiple and subsequent waves of CDRs, significantly reduced persistent motility (indicated as directionality) and altered mean velocity (Fig. 4C). These latter observations are consistent with the possibility that multiple and short lived CDRs are induced by the expression of the transgene, leading to cells that frequently change the direction of their protrusions and motion, and cannot persistently move in a biased direction. To further substantiate this notion, we analyzed the migratory behavior of control and RAB35-silenced MEFs moving along a PDGF gradient through an array of pillars where directional decision choices must be made. The array is composed of pillars from a photocurable hybrid polymer separated by a 4-micrometer space (Fig. 4D). Control cells navigate toward the PDGF gradient by extending persistent migratory protrusions, most of which were oriented coherently with the direction of the gradient. Conversely, loss of RAB35 reduces significantly chemotaxis and the number of cells with protrusions oriented along the gradient (Fig. 4D).

Finally, if our model were correct, we would expect that RAB35 loss might not be strictly required for migration toward stimuli that poorly or do not induce CDRs formation. Consistently, we showed that RAB35 loss inhibited chemotaxis of MEFs toward serum, which poorly induces CDR formation, much less drastically than toward PDGF (Fig. S2A-B). Additionally, RAB35 was dispensable for chemotactic migration toward EGF, which is unable to induce the formation of CDRs in MEFs (Fig. S2C-D). Similarly, RAB35 loss had no effect on MEFs migration in scratch wound assays. Under these latter conditions, cells migrate by kenotaxis without forming CDRs, while extending lamellipodia and filopodia protrusions like control cells (Fig. S2E and Movie 9).

RAB35 is required for chemoinvasion.

Collectively, our findings argue that deficiency in CDR formation leads to a slight impairment in cell locomotion but a more dramatic inhibition of directional sensing and chemotactic-guided migration further impacting on cell persistence, at least during crawling locomotion on 2D surfaces typically measured by all these assays. *In vivo*, however, cell migration occurs within complex 3D matrices with different structural organization, fibres composition and physical properties. Under these conditions, cells frequently move along single ECM fibres or narrow channels that impose a defined, physical confinement. To this end, we performed migratory assays on 1D micro-printed as well as suspended ECM lines. These assays mimic 1D tumour interstitial migration and allow, through the live monitoring of cell motion, a precise control of migratory parameters. Using suspended fibres, we showed that RAB35 ablation impeded the crawling mode of locomotion. Cells devoid of RAB35 were no longer able to extend trains of expanding wave and were stuck on the fibres (Movie 10). Next, to provide a more reliable quantitation of this phenotype, we turned to 1D micro-printed fibronectin tracks. We seeded MEF shCtrl and shRAB35 cells on lines of 10 microns in width and monitored their 1D locomotion by time-lapse phase contrast microscopy for 24 hours. Cell trajectories were automatically reconstructed by a build in-house ImageJ macro and a number of migratory parameters were extrapolated. Results showed that the absence of RAB35 affected cell velocity, the total length covered and, more relevantly, the persistence of cell motion (Fig. 5A and Movie 11).

Next, we wondered whether this protein might also play an active role in tumour cell dissemination in 3D matrix. To address this point, we tested MCF10.DCIS.com cells stably down-regulated for RAB35 in a set of *in vitro* migratory/invasive assays. This cell line is an oncogenic variant of MCF-10A that is widely used to recapitulate the transition from an *in situ* ductal to an invasive breast carcinoma [29, 30]. We first measured the ability of RAB35-depleted cells in migrating through a microporous membrane towards an HGF gradient in a Boyden chamber assay. Ablation

of RAB35 profoundly affected the chemotactic migratory ability of MCF10.DCIS.com cells (Fig. 5B). In addition, we also observed that control cells displayed a higher ability to invade and migrate through a thin layer of Matrigel in comparison to RAB35-down-regulated cells, as shown in the Matrigel invasion assay (Fig. 5C). To further validate this findings, we monitored by time-lapse phase contrast microscopy the invasive migration of control and RAB35-depleted MCF10.DCIS.com cells into 3D gels of native type I collagen enriched with the motogenic factors HGF [31-33]. Control cells readily invaded the 3D matrix. Conversely the chemoinvasive potential of RAB35-deficient cells was impaired as demonstrated by the reduced invasive forward index and cell velocity (Fig. 5D and Movie 12). Finally, we exploited the ability of MCF10.DCIS.com cells to generate invasive outgrowths in 3D basement membrane [34]. Control and RAB35-silenced MCF10.DCIS.com cells were seeded as single cells onto a gel composed of Matrigel and type I collagen and allowed to form spheroids. The addition of HGF in the presence of collagen type I is known to trigger an invasive program, characterized by the outgrowths of multicellular structures that expand from the regular contour of the spheroids [35]. This transition recapitulates what seen *in vivo* when *in situ* ductal carcinoma, confined into the lumen of a duct, convert into invasive ductal carcinoma through the extension of local multicellular protrusions [35]. The percentage of acinar structures that form invasive outgrowths was significantly reduced in RAB35-depleted cells (Fig. 5E), reinforcing the notion that RAB35 is necessary to promote a mesenchymal program of chemotactic cell invasion *in vitro*.

A RAB35/p85-PI3K axis mediates the chemotactic response to PDGF.

What are the cellular processes and molecular pathways RAB35 uses to promote CDR and steer cells in response to chemotactic stimuli?

To address this question, we initially turned to the well-established functional role of RAB35 in controlling clathrin-dependent endocytic internalization and membrane trafficking. More specifically, we tested the possibility that manipulation of RAB35 levels would impact on the trafficking of growth factor receptors, focusing on PDGFRB. However, no difference in either total PDGFRB or surface amounts could be found following silencing (Fig. S3A), or ectopic up-regulation (Fig. S3B) of RAB35.

We next utilized a molecular epistasis approach to position RAB35 action on known pathways controlling CDRs [7]. We have previously shown that the formation of these structures requires an active PDGFR, that function as first line sensor and transducer of PDGF signalling, and a functional endosomal trafficking route, in turn, necessary to spatially restrict RAC1-activity and RAC1-dependent actin remodelling into CDR[8], defining an epistatic relationship between these

components (Fig. 6A). To position RAB35 along this pathway, we exploited the finding that elevation of the levels of this protein is sufficient to promote multiple CDRs in the absence of GF. Specifically, we monitored by time-lapse phase contrast microscopy the dynamics of CDRs in MEF cells silenced for *Pdgfrb*, or *Rab5a, b and c* or *Rac1* in control (-DOX) and doxycycline–inducible, RAB35-expressing populations (+DOX). The number and dynamics of CDR formation, as expected, was robustly increased upon elevation of RAB35 levels. The silencing of PDGF Receptor had no effects on CDR, consistently with the notion that elevation of RAB35 is sufficient to bypass the need of ectopic addition of GF to induce these protrusions. On the contrary, silencing of *Rab5* or *Rac1* genes nearly completely abrogated RAB35-induced CDRs (Fig. 6B and Movie 13). Thus, RAB35 appears to act down-stream of PGDF Receptor and either up-stream or in a parallel RAB5/ RAC1-pathway.

To investigate further this latter possibility and gain a molecular understanding of the mechanisms of action of RAB35, we systematically silenced all, the so far-identified, molecular effectors (Ocrl, Rusc2, Acap2, Mical1, Micall1, Fscn1 and p85) as well as guanine nucleotide exchange factors (Dennd1a, Dennd1b, Dennd6b and Flc) of this GTPase [36, 37]. MEF cells were systematically down-regulated for the indicated genes [only in the case of p85 we used MEFs double KO of the two isoforms p85 [38] instead of performing the transient down-regulation of the genes], serum-starved for 2 hours, stimulated with PDGF and scored for the ability to form CDRs. The resulting CDR-score showed that the genetic ablation of p85 isoforms was the sole manipulation able to phenocopy the loss of RAB35 (Fig. 6C). The lack of effects of critical downstream effectors mediating RAB35 known role as modulator of endocytosis further strengthened the notion that this function may not be the one used to control CDR formation.

To provide evidence of a direct causal link between p85/PI3K axis and RAB35, we performed three sets of experiments. Firstly, we inhibited PI3K activity, which strictly depends on its association with the regulatory subunit p85α and p85β, using a pharmacological inhibitor. Treatment of PDGF-stimulated with LY294002 or the more specific GDC-0941 PI3K inhibitors, the efficacy of which was tested by measuring the phosphorylation levels of the PI3K target and effector protein AKT, severely abrogated the formation of CDRs (Fig. S4A-B). Inhibition of AKT with MK-2206 had, instead, no effect on PDGF-induced CDRs formation nor on macropinocytosis (Fig. S4C). More importantly, pharmacological inhibition of PI3K also effectively abrogated CDRs induced by the sole expression of RAB35 (i.e. in the absence of PDGF addition) (Fig. 7A and Movie 14). We corroborated the latter findings using MEF-KO for p85α and β. These cells and the related control cells were engineered to express RAB35 in a doxycycline-inducible fashion and monitored by time-lapse phase contrast microscopy. Removal of p85α and β completely prevented

the formation of highly dynamic CDRs induced by RAB35 expression (Fig. 7B and Movie 15). Finally, we tested biochemically whether RAB35 acts by directly modulating p85/PI3K activity. Indeed, while we were working on this project, RAB35 was identified as a critical and direct activator of the p85/PI3K-AKT pathway, shown to directly interact with the regulatory p85α subunit and to mediate, through this pathway, cell transformation [39]. In agreement with this latter finding, we found that: i) silencing of RAB35 reduced significantly the phosphorylation of AKT in response to PDGF stimulation, without affecting PDGFR phosphorylation status, and PDGFR-dependent MAPK activity (Fig. 7C); ii) the ectopic expression of RAB35, in doxycycline-stimulated MEF pSLIK HA-RAB35 cells cultured in growing conditions without addition of growth factors, caused the hyper-activation of AKT signaling without affecting the phosphorylation levels of other transducers (Fig. 7D); iii) RAB35 and p85α co-immunoprecipitated. This interaction was enhanced upon growth factors (GFs) stimulation. Importantly, wild type RAB35, but not an inactive dominant negative RAB35S22N mutant, associated with endogenous p85α, whereas dominant active RAB35 interacted with p85α in a constitutive growth factors-independent fashion (Fig. 7E-F). These latter findings imply that stimulation with growth factors might increase RAB35-GTP levels, leading to the activation of p85/PI3K pathway. Consistent, with this notion a dominant negative RAB35S22N mutant abrogated PDGF-induced CDRs formation and directional migration (Fig. S4D), whereas two recently identified activated, tumor-associated RAB35 mutants, *RAB35*A151T and F161L [39], promoted CDRs formation and elevated AKT phosphorylation in the absence of growth factor stimulation (Fig. S4E and Movie 16). iv) There is a correlation between the levels of RAB35 and of phosphoAKT in prostate cancer cell lines (Fig. S5A-B). Of note, the analysis of the TCGA data set indicated that RAB35 display a significant elevated copy number variation in about 16% of human prostate cancers (Fig. S5C). The variable expression of RAB35 was also observed across a panel of human prostate cancer in a Tissue Microarray (TMA) with 12/56 (21.4%) adenocarcinoma displaying elevated levels of RAB35 (score ≥ 1.5). Whereas only 2/32 (6%) of normal prostate tissues displayed RAB35 scores = 1.5 (Fig. S5D). These latter results indicate that deregulation of the levels of this GTPase may be positively selected in a subset of prostate tumors.

CONCLUSION

How cells respond to chemotactic cues and more specifically how they interpret relative shallow gradients frequently embedded in a highly noisy environment is an issue that has long been fascinated cell biologists. One emerging law in chemotaxis is that cells to precisely guide their motion must make use of excitable, self-oscillating systems [24, 40]. Actin-based migratory protrusions that randomly oscillate extending radially in crawling locomotory cells [41-43] or centrifugally expanding, ventrally-restricted actin-rich waves in neutrophil abide to this basic rule [25, 44, 45]. These oscillating systems can, in addition, be biased to form in recurrent and polarized fashion in response to chemotactic cues [24, 40].

CDRs have also been proposed to displays similar features [7, 22, 46]. Indeed, mathematical and biophysical models support the notion that the growth and decay of CDR actin can be explained as pulse propagation in an excitable media, in which a wave is able to propagate in a nonlinear dynamical system, which is the excitable media [7, 46]. However, whether CDRs are linked to chemotactic directional motility and the molecular determinant driving their kinematics has remained, by and large, elusive. Here, we provide evidence that the small RAB35 GTPase is necessary and sufficient to control the formation of CDRs and promote their oscillating, recurrent dynamic behaviors (Fig. S6-cartoon). We showed that the elevation of RAB35 is sufficient to induce the formation of multiple CDRs that expand centrifugally, travel along elongated protrusions, frequently in the form of oscillating waves, that precede or accompany the extension of lamellipodia protrusions. Stimulation with growth factors, including PDGF in fibroblast and HGF in epithelial cells, biased this behavior, virtually hijacking this excitable system for efficient chemotactic motility. Not surprisingly, RAB35 is essential for chemotaxis in 2D, directional locomotion in 1D and chemoinvasion in 3D in various cellular systems.

Intriguingly, at the molecular levels, RAB35 controls the activity of an extensively studied chemotactic p85/PI3K axis [47, 48] (Fig. S6 scheme). The absolute requirement of this axis in chemoguidance remains somewhat controversial. Nevertheless p85/PI3K signaling node has been involved both in initiating as well as in biasing and stabilizing branched protrusions, which have been proposed to form stochastically, depending on cellular context [48, 49]. In the case of CDRs formation, the functional requirement of PI3K has long been established [50-52], and analysis of its activity and of coupled lipid-phosphatases have revealed how this axis generate a complex spatiotemporal dynamics of phosphatidylinositol-3,4,5-trisphosphate and its derivate products phosphatidylinositol 4,5-trisphosphate precisely along the membrane confining CDRs [51, 53]. This finding supports the notion that intrinsic PI3K-based feedback mechanisms control the duration, extent and the spatial choreography of phospholipids, in turn necessary to modulate the kinematics

of CDRs. Within this context, RAB35, which naturally cycles between inactive and active GTP, appears to be perfectly suitable to act as a locally excitable GTPase that directly impinges onto PI3K signalling network, ultimately tuning its activity in a growth factors-dependent fashion. A corollary of this tenet is that RAB35 should be locally accumulating in CDRs, as we showed, and its activity might be spatially restricted at these sites. Whether this is the case, and the additional factors modulating RAB35 activity remains to be established. Nevertheless, collectively, our findings reveal that RAB35 is a novel key molecular component of an oscillating, excitable network required to set the steering compass of chemotactically migrating cells (Fig. S6).

RAB35 has recently been shown to be a potentially oncogenic RAB protein [39]. This function was shown to be mediated by the ability of RAB35 to regulate a p85/PI3K-AKT axis, which, in turn, impinges onto PDK1 and mTORC2 pathways [39]. Consistently, two somatic RAB35 mutations found in human tumors generate alleles that constitutively activate PI3K/AKT signalling, suppress apoptosis, and transform cells in a PI3K-dependent manner [39]. Our finding indicates that RAB35 and the oncogenic-associated mutant forms are also implicated in CDR formation and chemotactic migration in a AKT–independent, but PI3K-dependent fashion. These results argue that certain tumors might specifically exploit and select for alterations of RAB35 also to increase their invasiveness and ability to navigate through complex interstitial environment. We further showed that RAB35 elevation is sufficient to enhance macropinocytosis. This process has recently emerged as a major scavenging route for proteinaceous material and lipid sources in order to refill the amino acid pools, fuel mitochondrial metabolism and lipid biosynthesis, particularly in tumors bearing K-RAS or PI3K activating mutations [54, 55], ultimately enabling survival in a nutrient-deprived tumor microenvironment. Thus, RAB35 might not only be important for the onset of tumorigenesis, but also to increase nutritional tumor adaptation and progression, possibly by promoting tumor dissemination potential.

FIGURE LEGENDS

Figure 1. siRNA-based screening for RAB GTPases indispensable for PDGF-induced CDRs formation

(A) Primary screening results. siRNAs targeting RAB GTPases were ranked according to their CDR-score (see methods and Fig. S1). Representative images of positive (si*Pdgfrb*) and negative (siEGFP) controls are respectively in red and green. siRNAs best inhibiting CDR formation (more than 60% reduction relative to scrambled siEGFP) are enclosed into the light grey box. The oligo s95003 targeting *Rab35*, indicated in blue, is reported as representative example. Red arrows indicate CDRs. Scale bar, 50 µm.

(B) The siRNAs that inhibited CDRs formation more efficiently were validated in a completely independent experiment. *Left*: MEF cells interfered for *Rab35* (ID: s95002, s95003), or *Rab8a* (ID: s69778, s69779), or *Rab8b* (ID: s108154, s108155, s108156), *Pdgfrb* (positive control) or Scrambled oligo (negative control). Upon PDGF stimulation, cells were fixed and stained with phalloidin. Representative images are shown for each experimental condition. Red arrows indicate CDRs. Scale bar, 50 µm. *Right*: CDRs were manually counted and normalized against scrambled-transfected, control samples. Data are the mean ± SD (n > 200 cells/condition in 3 independent experiments). The silencing of the targeted genes was verified by qRTPCR.

Figure 2. RAB35 critically affects the formation of CDRs

(A) Expression of siRNA-resistant human RAB35 rescues CDRs formation. Doxycycline-treated pSLIK-HA-RAB35 (human) infected MEFs were silenced for endogenous RAB35, serum-starved for 2 hours, stimulated with PDGF for 10 minutes and fixed. Samples were co-stained with FITC-Phalloidin and the anti-HA antibody to detect F-actin and human HA-RAB35 transgene expression, respectively. Red arrows indicate CDRs. Scale bar, 50 µm. CDR-score was calculated by normalizing the number of CDR-positive cells per each condition against the scrambled doxycycline-untreated and PDGF-stimulated sample, used as control. Data are the mean ± SD (n > 100 cells/condition in 3 independent experiments). The silencing of endogenous RAB35 was verified by qRTPCR.

(B) Silencing of RAB35 impairs macropinocytosis. MEF control (shCtrl) and *Rab35*-downregulated (sh*Rab35*) cells were serum starved for 2 hours and incubated (+) or not (-) for 1 hour with PDGF and tetramethylrhodamine-dextran. Upon fixation, cells were processed for epifluorescence analysis to identify nuclei (blue) and TMR-dextran-positive macropinosomes (red), respectively. Scale bar, 20µm. In the bottom graph, quantification of dextran uptake was performed by determining the total cell fluorescence/cell (see methods) expressed as arbitrary units. Data are the mean ± SD (n= 40

cells/condition in 3 independent experiments). **p < 0.01; *p<0.05. The downregulation of RAB35 was assessed by qRTPCR analysis.

(C) RAB35 is sufficient to induce the spontaneous formation of CDRs. MEF control (Ctrl), HA-RAB35-expressing (HA-RAB35) and *Rab35*-silenced (si*Rab35*) cells were monitored for 1 hour by time-lapse phase contrast microscopy in the absence of any added PDGF. Still phase contrast images from time-lapse sequence (Movie 2) are shown. Red arrows indicate CDRs. Scale bar, 50 µm. The number of CDRs/cell formed in 1 h is expressed as mean ± SEM (n = 60 cells/condition in three independent experiments). ****p < 0.0001, paired Student's t-test. The levels of RAB35 mRNA were determined by qRTPCR.

(D) RAB35 expression promotes macropinocytosis in the absence of GFs. Doxycycline-treated pSLIK-HA-RAB35 (human) infected MEFs were incubated for 1 hour with TMR-dextran. Upon fixation, images were processed for epifluorescence to visualise nuclei (blue), TMR-dextran-positive macropinosomes (red) and the ectopic expression of HA-RAB35 protein (green). Quantification of dextran uptake performed as described in B. The total fluorescence/cell was expressed as arbitrary units. Scale bar, 20 µm. Data are the mean ± SD (n= 40 cells/condition in 3 independent experiments). *p<0.05.

Figure 3. Kinematics of CDRs

(A) CDRs formation anticipates the extension of protrusion with a typical lag phase in response to a local gradient of PDGF. *Top*: Still images from a representative time-lapse sequence (Movie 3) of MEF cells stimulated by the local delivery of PDGF using a micropipette. The formation of CDRs and subsequent protrusions extensions were monitored by time-lapse phase contrast microscopy. Images were acquired every 20 seconds for 20 minutes. The position of PDGF release is indicated by the grey arrow. Red and white arrows indicate CDR and protrusions extension, respectively. The white dashed line indicates the ROI used to perform the kymograph shown on the bottom right panel. Scale bar, 20µm. *Bottom left*: cartoon depicting the dynamics of CDRs and protrusions. *Bottom right*: kymograph of leading edge dynamics. PDGF stimulation (T_0), CDR closure time (T_1) and protrusion extension (T_2), times are indicated on the left.

(B) RAB35 promotes the formation of multiple CDRs that expand centrifugally and precede the extension of leading edge protrusions. *Top*: pSLIK-HA-RAB35 (human)-MEFs were infected with EGFP-LifeAct and treated or not with doxycycline to induce the transgene expression. Samples were monitored by time-lapse fluorescence microscopy every 30 seconds for a period of 1 hour. Still images from time-lapse sequence (Movie 4) are shown. Scale bar, 50 µm. Boxes indicate magnified areas shown on the side (Scale bar, 20 µm). Red and white arrows indicate CDRs and

protrusion extension, respectively. *Bottom left*: the lag phase between CDR closure and the subsequent protrusion extension, was quantified and reported as mean ± SD (n = 30 cells/experiments out of 3 independent experiments). *Bottom right*: RAB35 ectopic expression was assessed by WB analysis.

(C) RAB35 induces the formation of travelling CDR waves. *Top*: pSLIK-HA-RAB35 (human)-MEFs were infected with EGFP-LifeAct and treated or not with doxycycline to induce the transgene expression. Samples were monitored by time-lapse fluorescence microscopy every 30 seconds for a period of 20 minutes. Still images from time-lapse sequence (Movie 5) are shown. Scale bar, 50 µm. The dashed line indicates the ROI used to perform the kymograph analysis. *Middle*: kymograph of cell edge dynamics. Blue and red lines follow the movements of the leading edge of a protrusion and a travelling CDR in the kymograph. *Bottom*: the movement of the CDR (red) and the protrusion at the leading edge (blue), obtained upon RAB35 ectopic expression, was measured by plotting the distance travelled overtime. Velocities are reported as mean ± SD (n = 30 cells out of 3 independent experiments).

(D) RAB35 promotes recurrent oscillating CDR waves. Doxycycline-treated pSLIK-HA-RAB35 (human)- EGFP-LifeAct-expressing MEFs were imaged every 30 sec for 1 hour period. Still fluorescence images from time-lapse sequence (Movie 6) are shown. Red arrows point the recurrent CDR formation. Scale bar, 10µm. A typical, representative frequency of recurrent waves was shown by profiling the mean fluorescence intensity of the GFP signal overtime. Peaks are indicated by red arrows and correspond to CDR formation.

Figure 4. RAB35 is required for optimal directional motility and chemotaxis

(A) Scrambled and *Rab35*-silenced MEFs were seeded into the upper chamber of 8-µm pore transwell, uncoated filters. PDGF (20 ng/ml) was added to the lower chamber. A subset of transwells was stained with Crystal Violet three hours after seeding and the top of the microporous membrane was analysed to ensure that an equal number of cells attached to the filters regardless of the treatment. After 20 hours cells migrated to the lower side of the microporous membrane were stained with Crystal Violet and counted. To quantify the extent of chemotaxis we determined the average number of cells per field ± SD (at least 6 fields of view/condition were analysed). Gene silencing was verified by qRTPCR.

(B) Cell chemotaxis towards a PDGF gradient was monitored in control (shCtrl) and *Rab35*-silenced (sh*Rab35*) MEFs by time-lapse phase contrast microscopy. Images were acquired every 5 minutes for 24 hours (Movie 7). Individual cells were manually tracked and analysed by Chemotaxis Tool ImageJ software plugin. Velocity and forward migration index (corresponding in

this case to a chemotactic index) are shown in whiskers box plots. Solid horizontal line = median value; box outlines = 25 th – 75 th percentiles; whiskers = min and max values. ****p < 0.0001, paired Student's t-test. Stable silencing of RAB35 has been verified by Western blot analysis.

(C) MEF control (shCtrl), *Rab35*-silenced (sh*Rab35*) and HA-RAB35-expresing (HA-RAB35) cells were seeded sparsely in the absence of any diffusible gradient. Random cell migration was recorded by time-lapse phase contrast microscopy every 5 minutes over a 24 hours period (Movie 8). Cell locomotion was manually tracked and the following migratory parameters extrapolated: velocity; directionality (defined as the ratio between Euclidean distance and travelled distance. Mean ± SEM is reported in red (n > 40 cells/condition in one of three independent experiments with similar results). ****p < 0.0001; **p < 0.01; *p<0.05.

(D) Chemotactic migration of MEF control (shCtrl) and *Rab35*-downregulated (sh*Rab35*) cells through an array of pillars. *Left:* schematic representation of the chemotactic device. An array of 4µm inter-spaced micropillars which were laser-printed on a glass substrate was placed in the middle area of a sticky-Slide Chemotaxis chamber (Ibidi). Cells were seeded from the inlets of the "cell pool area" and once spread, a chemotactic gradient was created by adding PDGF into the "cell exit area" at a concentration of 20 ng/ml. Cell dynamics was monitored by time-lapse phase contrast microscopy every 10 minutes for about 24 hours. *Middle:* still images of the time-lapse sequence are shown. Orientation of cell protrusions is indicated by superimposed red (shCtrl) and blue (sh*Rab35*) arrows. Scale bar, 50 µm. *Top right:* Individual cells were manually tracked and analysed by Chemotaxis Tool ImageJ software plugin. Forward migration index (corresponding to migratory persistence towards the chemotactic gradient) is reported as mean ± SEM. *Bottom right:* the protrusion orientation angle (ϕ) of migrating cells, delimited by the protrusion extension and the direction of the PDGF gradient, was calculated at different time point of the time-lapse experiment and reported as mean ± SEM. Values of 0 and 90 indicate that protrusions are oriented along and parallel to the chemotactic gradient, respectively (n > 100 cells/condition in one of three independent experiments with similar results). ***p < 0.001, paired Student's t-test.

Figure 5. RAB35 is required for 1D migration and chemo-invasion in 3D.

(A) Migration of Control (shCtrl) and *Rab35*-silenced (sh*Rab35*) cells in 1D. MEFs were seeded on fibronectin-coated lines of 10-µm width and imaged by time-lapse phase contrast microscopy every 5 minutes over a 10 hours period. Still phase contrast images at the indicated time points from time-lapse sequence (Movie 11) are shown. Scale bar, 100µm. Cell trajectories were automatically reconstructed and velocity, effective length and change of direction frequency (corresponding to the migratory persistence) are shown in whiskers box plots. Solid horizontal line = median value; box

outlines = 25 th – 75 th percentiles; whiskers = min and max values. ****p < 0.0001; ***p < 0.001, paired Student's t-test.

(B) Chemotactic migration of control (shRNA Ctrl) and stably *Rab35*-silenced (shRNA *Rab35*) MCF10.DCIS.com cells. Cells were seeded into 8-µm pore transwell uncoated filter as in figure 4A and the capability of migrating in the presence or absence of an HGF gradient was assessed. The migration index was calculated by normalizing the average number of cells per field with respect to control cells in the absence of gradient. Data are reported as mean ± SD (at least 6 fields of view/condition were analysed). Gene silencing was verified by qRTPCR.

(C) The chemo-invasive ability of control and *Rab35*-depleted MCF10.DCIS.com cells was tested in Matrigel invasion assays. Cells were seeded into the upper chamber of Matrigel-coated transwell filters. HGF (100 ng/ml) was added to the lower chamber. After 20 hours, cells migrated through the Matrigel layer were fixed by PFA 4%, stained with Crystal Violet and the invasion index was calculated as the migration index in B. Data are mean ± SD (at least 6 fields of view/condition were analysed).

(D) An equal number of Control and *Rab35*-silenced MCF10.DCIS.com cells were placed on one side of a chamber slide in which 2.3 mg/ml of acid extracted–only type I collagen gel containing 100 ng/ml HGF and 100 ng/ml EGF was polymerized. Cell invasion was monitored by time-lapse phase contrast microscopy every 10 minutes over a 48 hours period. *Left*: still phase contrast images from time-lapse sequence (Movie 12) are shown. Invading cells are indicated by white arrows. Scale bar, 100µm. *Right*: Migration tracks of randomly picked individual cells invading toward the HGF/EGF gradient over 48 h are shown. Quantification of cell invasion was expressed as the mean forward invasion index and mean velocity. The analysis was conducted on at least 30 cells/experimental condition in three independent invasion assays. Data are mean ± SEM. ****p < 0.0001; ***p < 0.001.

(E) Control and *Rab35*-silenced MCF10.DCIS.com cells were grown on a thick Matrigel/type I collagen mixture (see methods) and overlaid with media containing 2% Matrigel. After the formation of 3D spheroid structures, cells were cultured in the presence (+) or absence (-) of HGF for additional 48 hours. Magnification of the boxed area shown on the right is delimited by broken lines. The percentage of 3D structures with invasive outgrowths was quantified. Data are mean ± SD (n = 60 spheroids/condition in two independent experiments). Scale bar, 400µm.

Figure 6. Molecules acting in concert with RAB35 to promote Dorsal Ruffles formation

(A) Schematic representation of the signalling pathway leading to CDR formation.

(B) RAB5 and RAC are required for RAB35-dependent CDR formation but PDGFRB is dispensable. pSLIK-HA-RAB35 (human)-MEFs were silenced for *Pdgfrb*, or *Rab5* or *Rac1* and

569 treated or not with doxycycline to induce the transgene expression. CDR formation was monitored
570 by time-lapse phase contrast microscopy every 30 seconds for 1 hour. Still phase contrast images
571 from time-lapse sequence (Movie 13) are shown. CDRs are indicated by red arrows. Scale bar,
572 100µm. The number of CDRs/cell/h was reported as mean ± SEM (at least 30 cells/condition in
573 each of the three independent experiments were analysed). ****p < 0.0001; ns not significant,
574 paired Student's t-test. The silencing of the targeted genes was verified by qRTPCR.
575 (C) Silencing of Rab35 GEFs or effectors. MEF cells were interfered for the indicated Rab35 GEFs
576 or effectors and tested for their ability in forming CDRs upon PDGF stimulation. Representative
577 Phalloidin-stained images are reported for each experimental condition. Scale bar, 50µm. CDRs
578 were manually counted and normalized against the scrambled sample. Data are the mean ± SD (n >
579 200 cells/condition in three independent experiments). ****p < 0.0001; **p < 0.01, paired
580 Student's t-test. The silencing of the targeted genes was verified by qRTPCR. In the case of p85,
581 double p85α and β KO MEFs [38] were employed and the loss of p85 isoforms was confirmed by
582 Western blotting. In the latter case, as control we used both p85α+/-p85β–/– MEFs (p85-/+,
583 derived from sibling mice) as well as p85α-/-p85β–/– MEF in which p85α was re-expressed.
584
585 **Figure 7. A RAB35/PI3K axis is necessary for triggering CDR formation**
586 (A) PI3K inhibition impairs RAB35-induced CDR formation. pSLIK-HA-RAB35 (human)-MEFs
587 were treated or not with doxycycline to induce the transgene expression and incubated with vehicle
588 or LY294002. Cells were imaged by time-lapse phase contrast microscopy every 30 seconds for 1
589 hour period. Still phase contrast images from time-lapse sequence (Movie 14) are shown. CDRs are
590 indicated by red arrows. Scale bar, 50µm. The number of CDR/cell is reported as mean ± SEM (n >
591 30 cells/condition out of three independent experiments). ****p < 0.0001, paired Student's t-test.
592 RAB35 ectopic expression was verified by IF.
593 (B) Genetic ablation of the regulatory subunits of PI3K abrogates the RAB35-dependent CDR
594 formation. Control MEF or p85α–/– pβ-/- double KO cells (p85-/-) [38] were infected with pSLIK
595 HA-RAB35 lentiviruses in order to express RAB35 in a doxycycline-inducible fashion. These cells
596 were cultured in the presence or absence of doxycycline without any supplement of growth factors
597 and imaged by time-lapse phase contrast microscopy every 30 sec for 1 h period. *Left*: Still phase
598 contrast images from time-lapse sequence (Movie 15) are shown. CDRs are indicated by red
599 arrows. Scale bar, 50µm. *Middle graph*: The number of CDR/cell is reported as mean ± SEM (n =
600 50 cells/condition in two independent experiments). ****p < 0.0001; *p<0.05, paired Student's t-
601 test. *Right graph*: RAB35 ectopic expression was verified by qRTPCR. Data are the fold increase of
602 RAB35 mRNA levels of doxycycline-treated with respect to untreated ones.

(C-D) RAB35 regulates AKT activity. (C) Control (shCtrl) and *Rab35*-silenced (shRab35) cells were serum starved for 2 hours and stimulated or not for 10 minutes with PDGF. Total cell lysates were analysed by Western blot to detect total or phosphorylated levels of the indicated proteins. Vinculin was used as loading control. (D) Lysates from pSLIK-HA-RAB35 (human)-MEFs treated or not wit doxycycline were immunoblotted as described in C.

(E) RAB35 co-immunoprecipitates with endogenous p85α. p85α–/– pβ-/- double KO cells (p85-/-) and control MEFs were serum starved for 4 hours and stimulated or not for 10 minutes with PDGF. Total cell lysates (1 mg) were immunoprecipitated with anti-p85α monoclonal antibody or irrelevant immunoglobulin G (IgG). Total cell lysates (50 µg) and immunoprecipitates (IPs) were immunoblotted with the indicated antibodies

(F). Active RAB35 interacts with p85α. HeLa cells were transfected with RAB35 WT, or RAB35 S22N or RAB35Q67L fused to EGFP. Upon 24 hours, samples were serum starved for 4 hours and mock treated (−) or stimulated with HGF (+) for 10 min at 37°C. Total cell lysates (1 mg) were immunoprecipitated with anti-p85α monoclonal antibody or irrelevant immunoglobulin G (IgG). Total cell lysates (50 µg) and immunoprecipitates (IPs) were immunoblotted with the indicated antibodies.

Acknowledgments

We thank Arnaud Echard for critically reading the manuscript and providing key RAB35 reagents. This work has been supported by the Associazione Italiana per la Ricerca sul Cancro (AIRC #10168 and # 18621), the International Association For Cancer Research (AICR-09-0582 & 14-0335); the European Research Council (Advanced-ERC#268836). SC and CM were supported by AIRC and Fondazione Umberto Veronesi fellowships, respectively.

Author Contribution

SC designed, performed and analysed data and wrote the paper; CM performed and analyzed data; BM and CT designed and developed software analysis tools for the imaging-based screening; AP and EF performed and developed assays of 3D cell migration; GME performed chemotactic assays; PN and PM performed, analysed microprinted-based migratory assays; AD performed cellular biochemical experiments: CG and NG performed, analysed suspended fibers assays; AF and MP designed and build the forest of pillars. GS designed, analyzed data and wrote the manuscript.

635 **Disclosure**

636 The authors declare no potential conflicts of interest.

637

REFERENCES

1. Friedl, P. & Alexander, S. Cancer invasion and the microenvironment: plasticity and reciprocity. *Cell* **147**, 992-1009 (2011).
2. Egeblad, M., Nakasone, E.S. & Werb, Z. Tumors as organs: complex tissues that interface with the entire organism. *Dev Cell* **18**, 884-901 (2010).
3. Ridley, A.J. Life at the leading edge. *Cell* **145**, 1012-1022 (2011).
4. Faix, J., Breitsprecher, D., Stradal, T.E. & Rottner, K. Filopodia: Complex models for simple rods. *Int J Biochem Cell Biol* **41**, 1656-1664 (2009).
5. Petrie, R.J., Gavara, N., Chadwick, R.S. & Yamada, K.M. Nonpolarized signaling reveals two distinct modes of 3D cell migration. *J Cell Biol* **197**, 439-455 (2012).
6. Paluch, E.K. & Raz, E. The role and regulation of blebs in cell migration. *Curr Opin Cell Biol* **25**, 582-590 (2013).
7. Hoon, J.L., Wong, W.K. & Koh, C.G. Functions and regulation of circular dorsal ruffles. *Mol Cell Biol* **32**, 4246-4257 (2012).
8. Palamidessi, A. *et al.* Endocytic trafficking of Rac is required for its activation and for the spatial restriction of signaling in cell migration. *Cell* **134**, 135-147 (2008).
9. Orth, J.D., Krueger, E.W., Weller, S.G. & McNiven, M.A. A novel endocytic mechanism of epidermal growth factor receptor sequestration and internalization. *Cancer Res* **66**, 3603-3610 (2006).
10. Gu, Z., Noss, E.H., Hsu, V.W. & Brenner, M.B. Integrins traffic rapidly via circular dorsal ruffles and macropinocytosis during stimulated cell migration. *J Cell Biol* **193**, 61-70 (2011).
11. Abella, J.V., Parachoniak, C.A., Sangwan, V. & Park, M. Dorsal ruffle microdomains potentiate Met receptor tyrosine kinase signaling and down-regulation. *J Biol Chem* **285**, 24956-24967 (2010).
12. Ruusala, A. *et al.* Platelet-derived growth factor (PDGF)-induced actin rearrangement is deregulated in cells expressing a mutant Y778F PDGF beta-receptor. *J Cell Sci* **111 (Pt 1)**, 111-120 (1998).
13. Mellstrom, K., Heldin, C.H. & Westermark, B. Induction of circular membrane ruffling on human fibroblasts by platelet-derived growth factor. *Exp Cell Res* **177**, 347-359 (1988).
14. Bernitt, E., Koh, C.G., Gov, N. & Dobereiner, H.G. Dynamics of actin waves on patterned substrates: a quantitative analysis of circular dorsal ruffles. *PLoS One* **10**, e0115857 (2015).
15. Roberts, M., Barry, S., Woods, A., van der Sluijs, P. & Norman, J. PDGF-regulated rab4-dependent recycling of alphavbeta3 integrin from early endosomes is necessary for cell adhesion and spreading. *Curr Biol* **11**, 1392-1402 (2001).
16. Araki, N., Hatae, T., Yamada, T. & Hirohashi, S. Actinin-4 is preferentially involved in circular ruffling and macropinocytosis in mouse macrophages: analysis by fluorescence ratio imaging. *J Cell Sci* **113 (Pt 18)**, 3329-3340 (2000).
17. Stenmark, H. Rab GTPases as coordinators of vesicle traffic. *Nat Rev Mol Cell Biol* **10**, 513-525 (2009).
18. Tang, B.L. & Ng, E.L. Rabs and cancer cell motility. *Cell motility and the cytoskeleton* **66**, 365-370 (2009).
19. Legg, J.A. *et al.* N-WASP involvement in dorsal ruffle formation in mouse embryonic fibroblasts. *Mol Biol Cell* **18**, 678-687 (2007).
20. Lanzetti, L., Palamidessi, A., Areces, L., Scita, G. & Di Fiore, P.P. Rab5 is a signalling GTPase involved in actin remodelling by receptor tyrosine kinases. *Nature* **429**, 309-314 (2004).
21. Sero, J.E., German, A.E., Mammoto, A. & Ingber, D.E. Paxillin controls directional cell motility in response to physical cues. *Cell Adh Migr* **6**, 502-508 (2012).

22. Doxzen, K. *et al.* Guidance of collective cell migration by substrate geometry. *Integr Biol (Camb)* **5**, 1026-1035 (2013).
23. Peleg, B., Disanza, A., Scita, G. & Gov, N. Propagating cell-membrane waves driven by curved activators of actin polymerization. *PLoS One* **6**, e18635 (2011).
24. Iglesias, P.A. & Devreotes, P.N. Biased excitable networks: how cells direct motion in response to gradients. *Curr Opin Cell Biol* **24**, 245-253 (2012).
25. Weiner, O.D., Marganski, W.A., Wu, L.F., Altschuler, S.J. & Kirschner, M.W. An actin-based wave generator organizes cell motility. *PLoS Biol* **5**, e221 (2007).
26. Diz-Munoz, A. *et al.* Membrane Tension Acts Through PLD2 and mTORC2 to Limit Actin Network Assembly During Neutrophil Migration. *PLoS Biol* **14**, e1002474 (2016).
27. Graziano, B.R. & Weiner, O.D. Self-organization of protrusions and polarity during eukaryotic chemotaxis. *Curr Opin Cell Biol* **30**, 60-67 (2014).
28. Wu, M. *et al.* Coupling between clathrin-dependent endocytic budding and F-BAR-dependent tubulation in a cell-free system. *Nat Cell Biol* **12**, 902-908 (2010).
29. Miller, F.R., Santner, S.J., Tait, L. & Dawson, P.J. MCF10DCIS.com xenograft model of human comedo ductal carcinoma in situ. *Journal of the National Cancer Institute* **92**, 1185-1186 (2000).
30. Hu, M. *et al.* Regulation of in situ to invasive breast carcinoma transition. *Cancer cell* **13**, 394-406 (2008).
31. Hotary, K.B. *et al.* Membrane type I matrix metalloproteinase usurps tumor growth control imposed by the three-dimensional extracellular matrix. *Cell* **114**, 33-45 (2003).
32. Sabeh, F. *et al.* Tumor cell traffic through the extracellular matrix is controlled by the membrane-anchored collagenase MT1-MMP. *J Cell Biol* **167**, 769-781 (2004).
33. Li, X.Y., Ota, I., Yana, I., Sabeh, F. & Weiss, S.J. Molecular dissection of the structural machinery underlying the tissue-invasive activity of membrane type-1 matrix metalloproteinase. *Mol Biol Cell* **19**, 3221-3233 (2008).
34. Lee, G.Y., Kenny, P.A., Lee, E.H. & Bissell, M.J. Three-dimensional culture models of normal and malignant breast epithelial cells. *Nature methods* **4**, 359-365 (2007).
35. Jedeszko, C., Victor, B.C., Podgorski, I. & Sloane, B.F. Fibroblast hepatocyte growth factor promotes invasion of human mammary ductal carcinoma in situ. *Cancer research* **69**, 9148-9155 (2009).
36. Klinkert, K. & Echard, A. Rab35 GTPase: A Central Regulator of Phosphoinositides and F-actin in Endocytic Recycling and Beyond. *Traffic* **17**, 1063-1077 (2016).
37. Chaineau, M., Ioannou, M.S. & McPherson, P.S. Rab35: GEFs, GAPs and effectors. *Traffic* **14**, 1109-1117 (2013).
38. Brachmann, S.M. *et al.* Role of phosphoinositide 3-kinase regulatory isoforms in development and actin rearrangement. *Mol Cell Biol* **25**, 2593-2606 (2005).
39. Wheeler, D.B., Zoncu, R., Root, D.E., Sabatini, D.M. & Sawyers, C.L. Identification of an oncogenic RAB protein. *Science* **350**, 211-217 (2015).
40. Shi, C., Huang, C.H., Devreotes, P.N. & Iglesias, P.A. Interaction of motility, directional sensing, and polarity modules recreates the behaviors of chemotaxing cells. *PLoS computational biology* **9**, e1003122 (2013).
41. Welf, E.S., Ahmed, S., Johnson, H.E., Melvin, A.T. & Haugh, J.M. Migrating fibroblasts reorient directionality by a metastable, PI3K-dependent mechanism. *J Cell Biol* **197**, 105-114 (2012).
42. Andrew, N. & Insall, R.H. Chemotaxis in shallow gradients is mediated independently of PtdIns 3-kinase by biased choices between random protrusions. *Nat Cell Biol* **9**, 193-200 (2007).
43. Insall, R.H. & Machesky, L.M. Actin dynamics at the leading edge: from simple machinery to complex networks. *Dev Cell* **17**, 310-322 (2009).

44. Millius, A., Dandekar, S.N., Houk, A.R. & Weiner, O.D. Neutrophils establish rapid and robust WAVE complex polarity in an actin-dependent fashion. *Curr Biol* **19**, 253-259 (2009).
45. Wu, M., Wu, X. & De Camilli, P. Calcium oscillations-coupled conversion of actin travelling waves to standing oscillations. *Proc Natl Acad Sci U S A* **110**, 1339-1344 (2013).
46. Zeng, Y., Lai, T., Koh, C.G., LeDuc, P.R. & Chiam, K.H. Investigating circular dorsal ruffles through varying substrate stiffness and mathematical modeling. *Biophys J* **101**, 2122-2130 (2011).
47. Gambardella, L. & Vermeren, S. Molecular players in neutrophil chemotaxis--focus on PI3K and small GTPases. *J Leukoc Biol* **94**, 603-612 (2013).
48. Afonso, P.V. & Parent, C.A. PI3K and chemotaxis: a priming issue? *Science signaling* **4**, pe22 (2011).
49. Yoo, S.K. *et al.* Differential regulation of protrusion and polarity by PI3K during neutrophil motility in live zebrafish. *Dev Cell* **18**, 226-236 (2010).
50. Wymann, M. & Arcaro, A. Platelet-derived growth factor-induced phosphatidylinositol 3-kinase activation mediates actin rearrangements in fibroblasts. *Biochem J* **298 Pt 3**, 517-520 (1994).
51. Hasegawa, J. *et al.* SH3YL1 regulates dorsal ruffle formation by a novel phosphoinositide-binding domain. *J Cell Biol* **193**, 901-916 (2011).
52. Tsujita, K. & Itoh, T. Phosphoinositides in the regulation of actin cortex and cell migration. *Biochim Biophys Acta* **1851**, 824-831 (2015).
53. Hogan, A. *et al.* The phosphoinositol 3,4-bisphosphate-binding protein TAPP1 interacts with syntrophins and regulates actin cytoskeletal organization. *J Biol Chem* **279**, 53717-53724 (2004).
54. Palm, W., Araki, J., King, B., DeMatteo, R.G. & Thompson, C.B. Critical role for PI3-kinase in regulating the use of proteins as an amino acid source. *Proc Natl Acad Sci U S A* **114**, E8628-E8636 (2017).
55. Commisso, C. *et al.* Macropinocytosis of protein is an amino acid supply route in Ras-transformed cells. *Nature* **497**, 633-637 (2013).

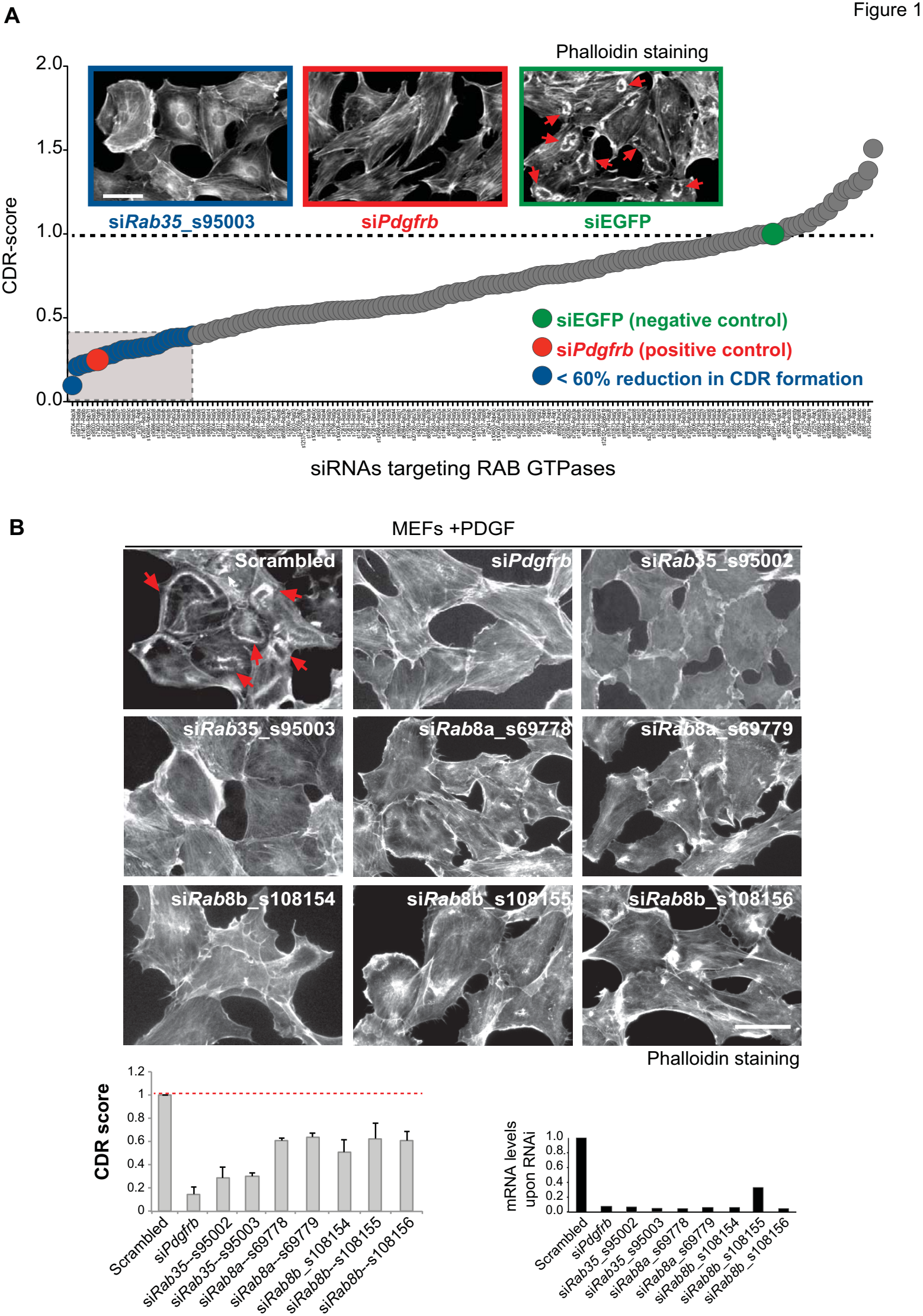
A
Phalloidin staining
2.0
1.5
1.0
0.5
0.0
CDR-score
siRab35_s95003
siPdgfrb
siEGFP
siEGFP (negative control)
siPdgfrb (positive control)
< 60% reduction in CDR formation
siRNAs targeting RAB GTPases
B
MEFs +PDGF
Scrambled
siPdgfrb
siRab35_s95002
siRab35_s95003
siRab8a_s69778
siRab8a_s69779
siRab8b_s108154
siRab8b_s108155
siRab8b_s108156
Phalloidin staining
CDR score
1.2
1
0.8
0.6
0.4
0.2
0
Scrambled
siPdgfrb
siRab35_s95002
siRab35_s95003
siRab8a_s69778
siRab8a_s69779
siRab8b_s108154
siRab8b_s108155
siRab8b_s108156
mRNA levels upon RNAi
1.0
0.8
0.6
0.4
0.2
0.0
Scrambled
siPdgfrb
siRab35_s95002
siRab35_s95003
siRab8a_s69778
siRab8a_s69779
siRab8b_s108154
siRab8b_s108155
siRab8b_s108156

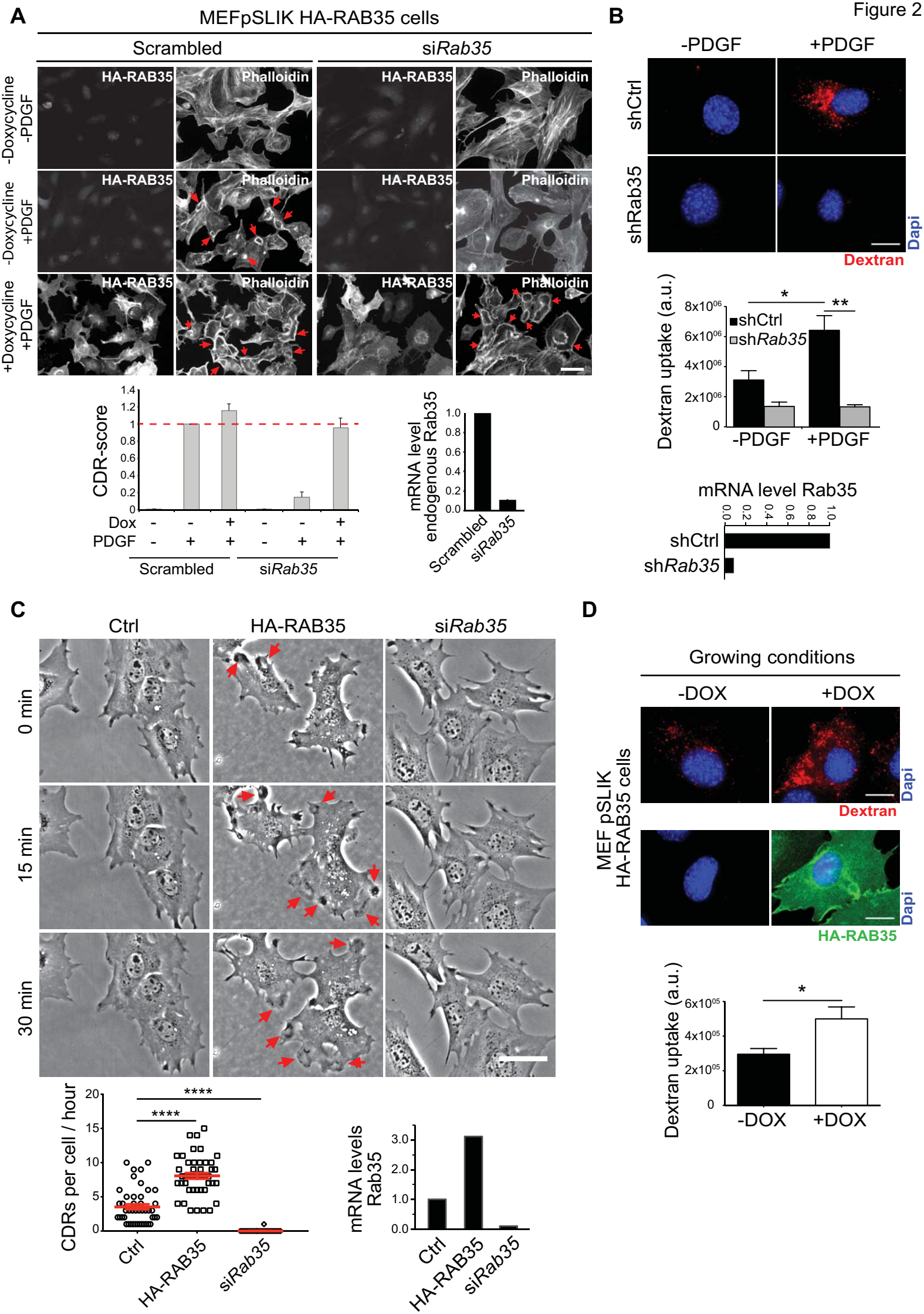
A
MEFpSLIK HA-RAB35 cells
Scrambled
siRab35
-Doxycycline -PDGF
-Doxycycline +PDGF
+Doxycycline +PDGF
HA-RAB35
Phalloidin
CDR-score
Dox
PDGF
Scrambled
siRab35
mRNA level endogenous Rab35
B
-PDGF
+PDGF
shCtrl
shRab35
Dapi
Dextran
Dextran uptake (a.u.)
shCtrl
shRab35
mRNA level Rab35
C
Ctrl
HA-RAB35
siRab35
0 min
15 min
30 min
CDRs per cell / hour
mRNA levels Rab35
D
Growing conditions
-DOX
+DOX
MEF pSLIK HA-RAB35 cells
Dapi
Dextran
HA-RAB35
Dextran uptake (a.u.)

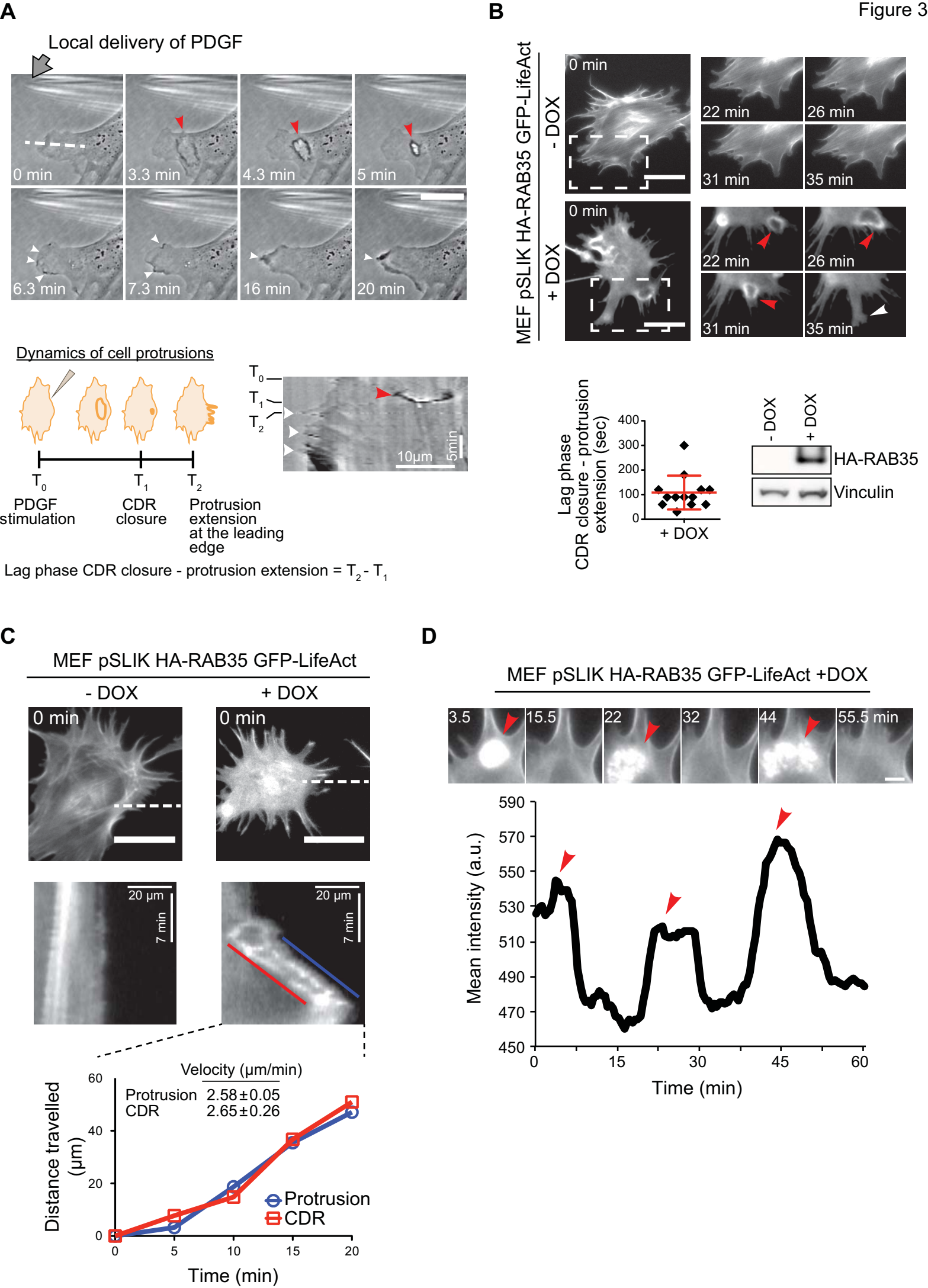
A
Local delivery of PDGF
0 min
3.3 min
4.3 min
5 min
6.3 min
7.3 min
16 min
20 min
Dynamics of cell protrusions
T0
T1
T2
PDGF stimulation
CDR closure
Protrusion extension at the leading edge
10μm
5min
Lag phase CDR closure - protrusion extension = T2 - T1
B
MEF pSLIK HA-RAB35 GFP-LifeAct
- DOX
+ DOX
0 min
22 min
26 min
31 min
35 min
Lag phase CDR closure - protrusion extension (sec)
400
300
200
100
0
+ DOX
- DOX
+ DOX
HA-RAB35
Vinculin
C
MEF pSLIK HA-RAB35 GFP-LifeAct
- DOX
+ DOX
0 min
20 μm
7 min
Velocity (μm/min)
Protrusion 2.58±0.05
CDR 2.65±0.26
Distance travelled (μm)
Protrusion
CDR
Time (min)
D
MEF pSLIK HA-RAB35 GFP-LifeAct +DOX
3.5
15.5
22
32
44
55.5 min
Mean intensity (a.u.)
Time (min)

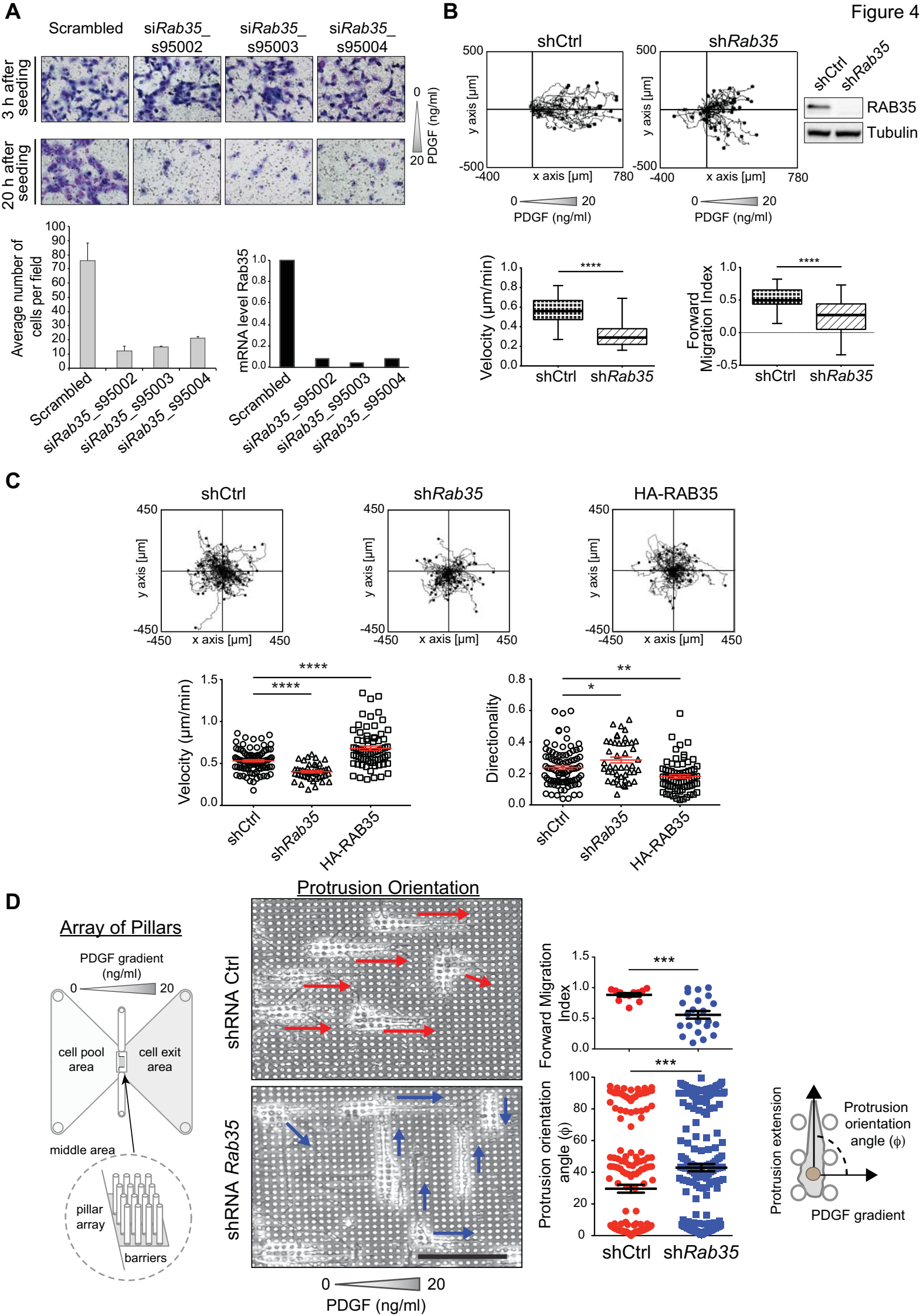
A
Scrambled
siRab35_ s95002
siRab35_ s95003
siRab35_ s95004
3 h after seeding
20 h after seeding
0
20
PDGF (ng/ml)
Average number of cells per field
mRNA level Rab35
Scrambled
siRab35_s95002
siRab35_s95003
siRab35_s95004
B
shCtrl
shRab35
y axis [µm]
x axis [µm]
PDGF (ng/ml)
RAB35
Tubulin
Velocity (µm/min)
Forward Migration Index
****
C
HA-RAB35
Directionality
*
**
***
D
Array of Pillars
PDGF gradient (ng/ml)
cell pool area
cell exit area
middle area
pillar array
barriers
Protrusion Orientation
shRNA Ctrl
shRNA Rab35
Protrusion orientation angle (ϕ)
Protrusion extension

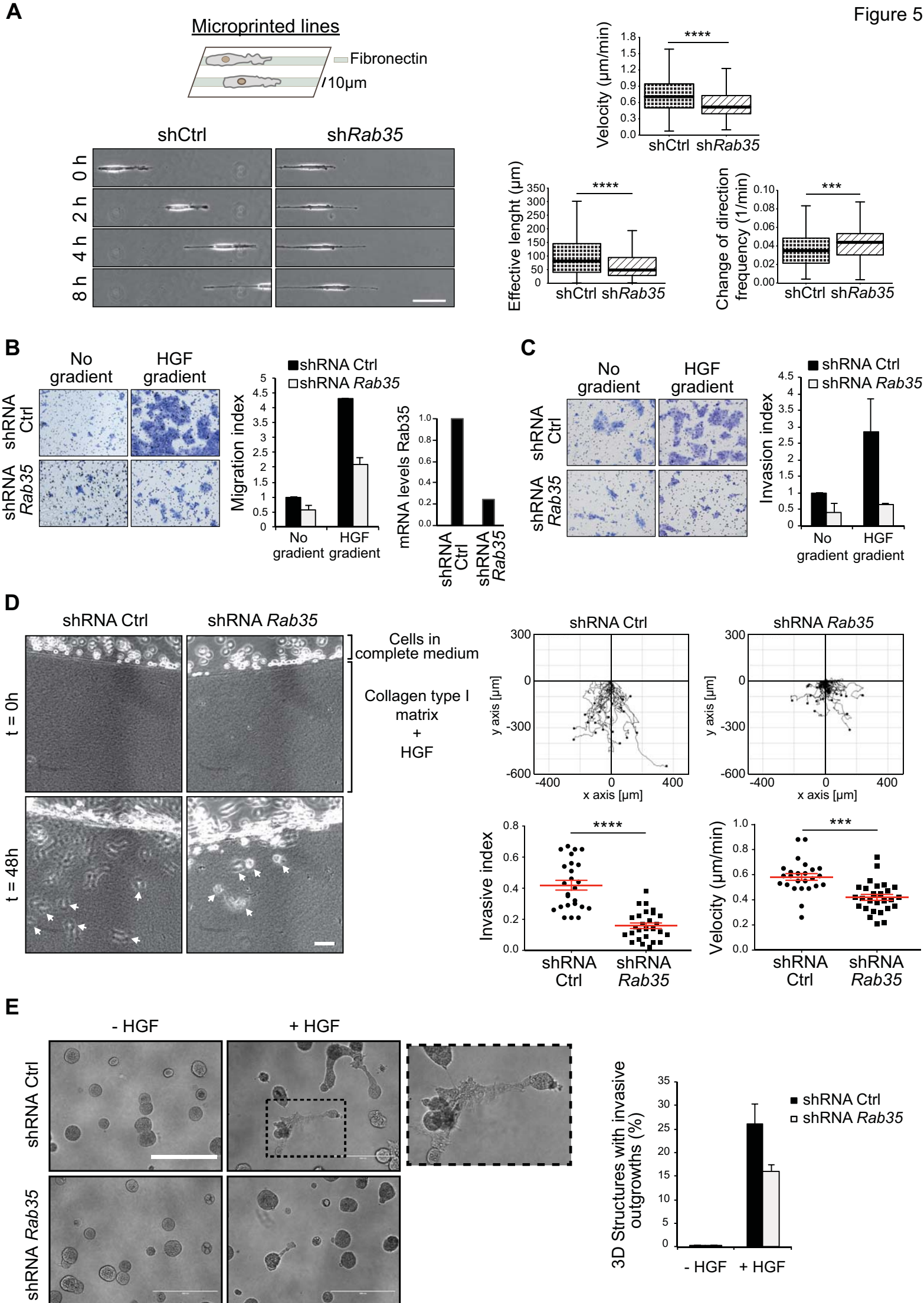
A
Microprinted lines
Fibronectin
/10µm
shCtrl
shRab35
0 h
2 h
4 h
8 h
Velocity (µm/min)
****
shCtrl shRab35
Effective lenght (µm)
****
shCtrl shRab35
Change of direction frequency (1/min)
***
shCtrl shRab35
B
No gradient
HGF gradient
shRNA Ctrl
shRNA Rab35
Migration index
shRNA Ctrl
shRNA Rab35
No gradient
HGF gradient
mRNA levels Rab35
shRNA Ctrl
shRNA Rab35
C
No gradient
HGF gradient
shRNA Ctrl
shRNA Rab35
Invasion index
shRNA Ctrl
shRNA Rab35
No gradient
HGF gradient
D
shRNA Ctrl
shRNA Rab35
t = 0h
t = 48h
Cells in complete medium
Collagen type I matrix + HGF
shRNA Ctrl
shRNA Rab35
y axis [µm]
x axis [µm]
Invasive index
****
shRNA Ctrl
shRNA Rab35
Velocity (µm/min)
***
shRNA Ctrl
shRNA Rab35
E
- HGF
+ HGF
shRNA Ctrl
shRNA Rab35
3D Structures with invasive outgrowths (%)
shRNA Ctrl
shRNA Rab35
- HGF
+ HGF

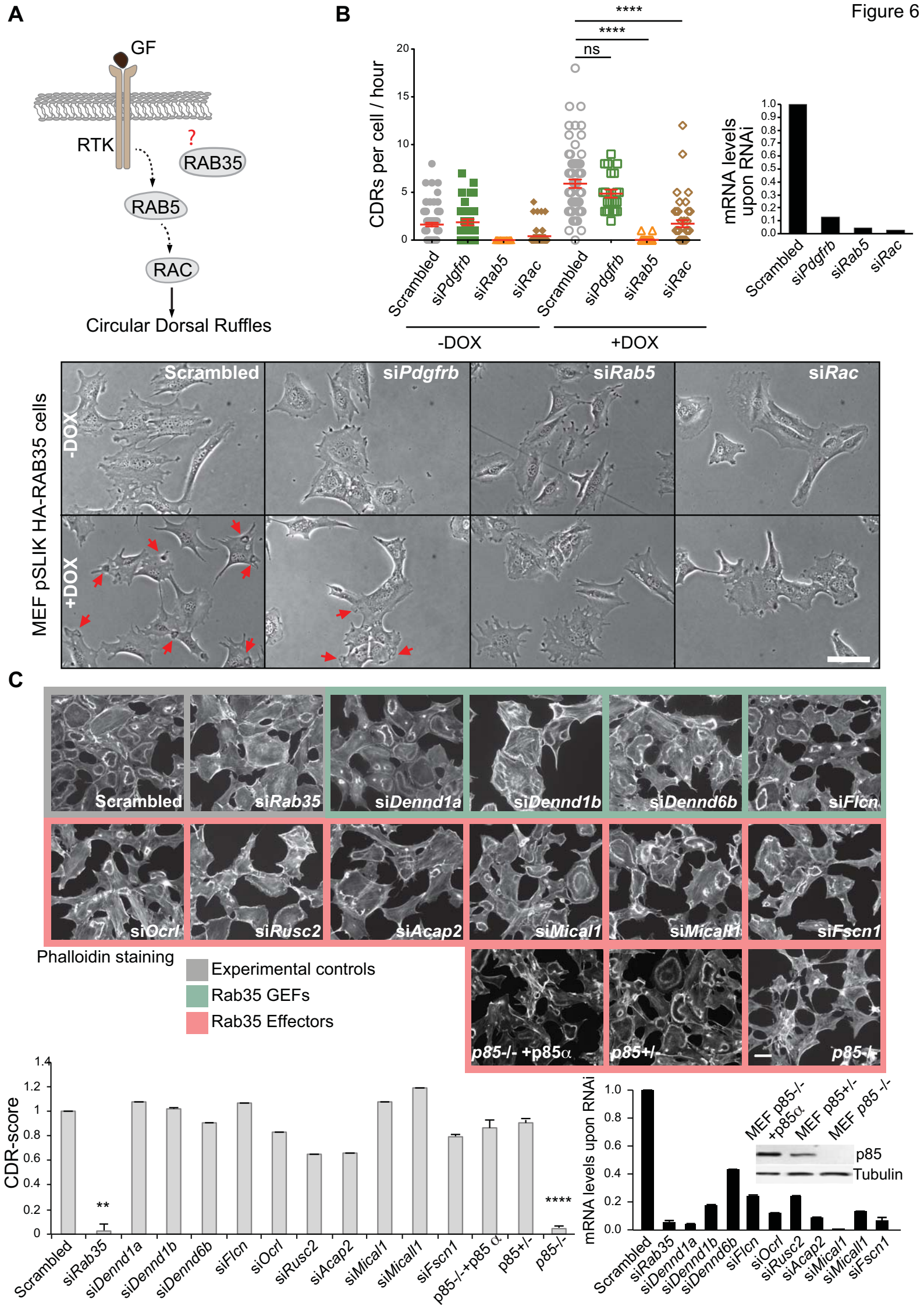
A
GF
RTK
?
RAB35
RAB5
RAC
Circular Dorsal Ruffles
B
CDRs per cell / hour
****
****
ns
Scrambled
siPdgfrb
siRab5
siRac
-DOX
+DOX
mRNA levels upon RNAi
MEF pSLIK HA-RAB35 cells
-DOX
+DOX
siRab35
siDennd1a
siDennd1b
siDennd6b
siFlcn
siOcrl
siRusc2
siAcap2
siMical1
siMicall1
siFscn1
Phalloidin staining
Experimental controls
Rab35 GEFs
Rab35 Effectors
p85-/- +p85α
p85+/-
p85-/-
C
CDR-score
**
****
p85-/-+p85 α
mRNA levels upon RNAi
MEF p85-/- +p85α
MEF p85+/-
MEF p85 -/-
p85
Tubulin

Figure 7

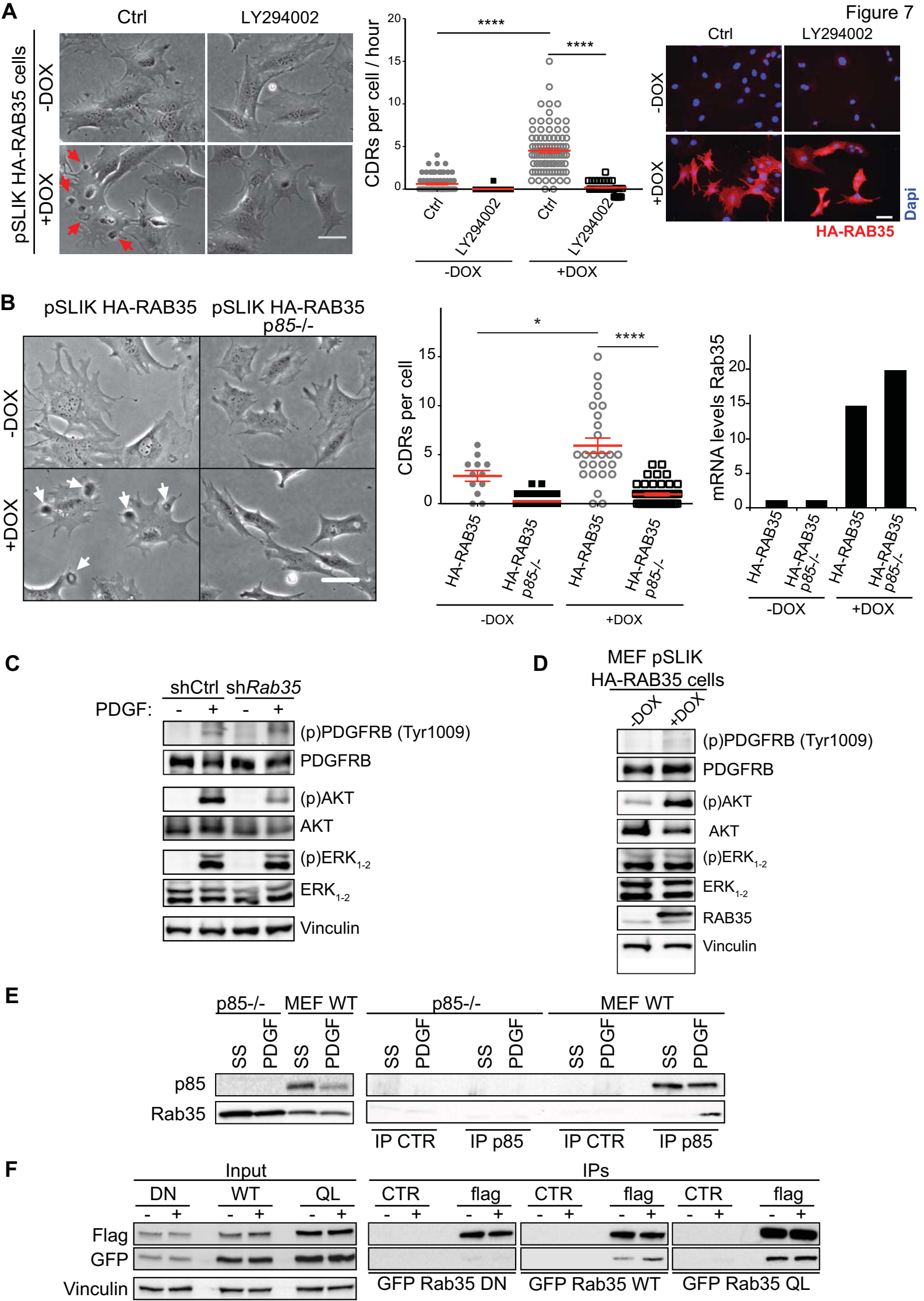
A
Ctrl
LY294002
pSLIK HA-RAB35 cells
-DOX
+DOX
CDRs per cell / hour
****
****
Ctrl
LY294002
Ctrl
LY294002
-DOX
+DOX
Ctrl
LY294002
-DOX
+DOX
Dapi
HA-RAB35
B
pSLIK HA-RAB35
pSLIK HA-RAB35 p85-/-
-DOX
+DOX
CDRs per cell
*
****
HA-RAB35
HA-RAB35 p85-/-
HA-RAB35
HA-RAB35 p85-/-
-DOX
+DOX
mRNA levels Rab35
HA-RAB35
HA-RAB35 p85-/-
HA-RAB35
HA-RAB35 p85-/-
-DOX
+DOX
C
shCtrl
shRab35
PDGF: - + - +
(p)PDGFRB (Tyr1009)
PDGFRB
(p)AKT
AKT
(p)ERK1-2
ERK1-2
Vinculin
D
MEF pSLIK HA-RAB35 cells
-DOX
+DOX
(p)PDGFRB (Tyr1009)
PDGFRB
(p)AKT
AKT
(p)ERK1-2
ERK1-2
RAB35
Vinculin
E
p85-/-
MEF WT
p85-/-
MEF WT
SS
PDGF
p85
Rab35
IP CTR
IP p85
IP CTR
IP p85
F
Input
IPs
DN
WT
QL
CTR
flag
CTR
flag
CTR
flag
Flag
GFP
Vinculin
GFP Rab35 DN
GFP Rab35 WT
GFP Rab35 QL